Electronic Supplementary Material (ESI) for Nanoscale.

Supporting Information for

UV-Trained and Metal-Enhanced Fluorescence of Biliverdin and Biliverdin Nanoparticles

Parinaz Fathi,[a] Ayman Roslend,[a] Kritika Mehta,[b] Parikshit Moitra,[c] Kai Zhang,[b] and Dipanjan Pan*[ad]

[a] Departments of Bioengineering, Materials Science and Engineering, and Beckman Institute
University of Illinois at Urbana-Champaign
Urbana, Illinois 61801, United States
[b] Department of Biochemistry, School of Molecular and Cellular Biology
University of Illinois at Urbana-Champaign
Urbana, Illinois 61801, United States
[c] Department of Pediatrics
University of Maryland School of Medicine
Health Sciences Facility III, 670 W Baltimore St, Baltimore, MD 21201
[d] Departments of Diagnostic Radiology Nuclear Medicine, Pediatrics, and Chemical and Biomolecular Engineering
University of Maryland School of Medicine and University of Maryland Baltimore County
Health Sciences Facility III, 670 W Baltimore St, Baltimore, MD 21201

Table of Contents

Materials

Biliverdin hydrochloride was purchased from Frontier Scientific. Cobalt (II) chloride was purchased from Alfa Aesar. Copper (II) chloride, iron (III) chloride, and manganese (II) chloride were purchased from Sigma Aldrich.

Methods

Biliverdin chelation and UV irradiation experiments

Biliverdin hydrochloride was dissolved overnight in 10 mL of water at a concentration of 1 mg/mL. Samples were protected from light unless otherwise noted. Prior to metal chelation, the pH of the biliverdin solution was raised to a pH of 10 using 1.0 M NaOH. A pH of 10 is commonly used for chelation of metals into biliverdin, and this high pH has been shown to allow for strong binding of biliverdin and bilirubin to metals without formation of any metal hydroxide precipitates.[1] We did not observe the formation of precipitates in these experiments. 500 µL of pH-adjusted biliverdin solution was placed in each 4-mL scintillation vial, and 50 µL of the corresponding metal chloride solution was added to each scintillation vial. Vials were shaken, after which the samples were either protected from light and placed under ambient conditions (-UV), or placed beneath a 365 nm UV lamp (VWR UV-AC Hand Lamp, Cat. # 89131-492, 115V-60Hz, 0.16 Amps) for 72 hours.

Metal chloride solutions

Metal chloride solutions were prepared by dissolving each metal salt for a final metal concentration of 2.306 mmol/mL.

Biliverdin nanoparticle synthesis

Biliverdin hydrochloride was dissolved overnight in 10 mL of NaCl solution (0.154 moles/Liter) at a concentration of 1 mg/mL. Samples were protected from light unless otherwise noted. 6.7 mg of 1-Ethyl-3-(3-dimethylaminopropyl)carbodiimide (EDC) and 4.0 mg of N-Hydroxysuccinimide (NHS) were then added and allowed to stir for 10 minutes. 3.5 µL 2 2'-(ethylenedioxy)bis(ethylamine) was then added to the solution to begin the reaction. BVNPs were allowed to form for 24 hours, after which they were dialyzed for a further 24 hours against 500 mL of NaCl solution (0.154 moles/Liter) in dialysis cassettes with a molecular weight cutoff (MWCO) of 10,000 kDa.

Biliverdin nanoparticle chelation and UV irradiation experiments

Metal chloride solutions for BVNPs were prepared as described above. Prior to metal chelation, the pH of the BVNP solution was raised to a pH of 10 using 1.0 M NaOH. 500 µL of BVNP solution was placed in each 4-mL scintillation vial, and 50 µL of the corresponding metal chloride solution was added to each scintillation vial. Vials were shaken, after which the samples were either protected from light and placed under ambient conditions (-UV), or placed beneath a 365 nm UV lamp (VWR UV-AC Hand Lamp, Cat. # 89131-492, 115V-60Hz, 0.16 Amps) for 72 hours.

UV-Visible Spectroscopy

UV-visible spectra were collected for wavelengths ranging from 230 nm to 900 nm using a Thermo Scientific Genesys 10S UV−Vis spectrophotometer. The baseline measurement was taken using 1 mL of water for BV samples, and 1 mL of NaCl solution (0.154 moles/Liter) for BVNP samples. Data was collected for a dilution of 10 µL of sample to 990 µL of diluent for BV samples, and 10 µL of sample to 990 µL of diluent for BVNP samples.

Fluorescence Spectroscopy

Fluorescence spectra were acquired for undiluted 100 µL samples of each type. Excitation wavelengths of 365 nm and 488 nm were used. Fluorescence spectra were collected on a TECAN infinite M200PRO.

Quantum Yield Calculations

Quinine sulfate and Rhodamine 6G were used to determine 365 nm and 488 nm quantum yield respectively. Quinine sulfate was dissolved at a concentration of 0.005 mg/ml in 0.1 M H_2SO_4. Rhodamine 6G was dissolved at a concentration of 10^{-7} mg/ml in water. The fluorescence spectra were collected for 100 µL undiluted samples of each type, while the absorbance spectra were collected at a dilution of 10 µL stock solution to 990 µL diluent. Quantum yield, Φ, was calculated using the following equation:

$$\Phi = \Phi_{ref} \times \left(\frac{I}{I_{ref}}\right) \times \left(\frac{1 - 10^{-A_{ref}}}{1 - 10^{-A}}\right) \times \left(\frac{\eta}{\eta_{ref}}\right)$$

Where I represents the integrated fluorescence intensity, A represents the absorbance at the selected wavelength, and η represents the solvent refractive index. The subscript "ref" indicates that the parameter is that of the reference dye. Average integrated fluorescence intensities across 3 trials were used for these calculations, along with average absorbances across 2 trials.

Stern-Volmer analysis on molecular biliverdin

100 X stock metal salt solutions were prepared by dissolving each metal salt at a concentration of 230.6 mmol/mL. 10 X, 1 X, 0.1 X, and 0.01 X solutions were prepared by diluting the 100 X stock solutions. 500 µL of pH-adjusted biliverdin solution was placed in each 4-mL scintillation vial, and 50 µL of the corresponding metal chloride solution was added to each scintillation vial. Vials were shaken, after which the samples were protected from light and chelation was allowed to occur for 72 hours. Afterwards, absorbance and fluorescence spectra were collected for the samples.

Fourier Transform Infrared Spectroscopy

FT-IR measurements were taken using the smart refractor accessory on a Thermo Nicolet Nexus 670 FT-IR. Samples were prepared by depositing the BV or BVNP solutions on Kevley MirrIR corner frosted FT-IR slides. Samples were dried under vacuum prior to collection of spectra.

Mass Spectrometry

Mass spectra were acquired using electrospray ionization (ESI) for m/z of 50 to 950 for BV samples, and 400 to 1500 for BVNP samples.

Circular Dichroism

Circular dichroism spectra were collected on a Jasco 710 CD spectrometer using a 2 mm quartz cuvette. Samples were diluted in water for these measurements, and multiple spectra were collected per sample.

Transmission Electron Microscopy

TEM images were acquired with an acceleration voltage of 200 keV on a JEOL Cryo 2100 TEM. Microscopy samples were prepared on 300-mesh to 400-mesh carbon-coated copper TEM grids. Samples were diluted (10 µL BVNP solution, 40 µL to 90 µL water). 2.5 µL of diluted solution was drop-cast onto each TEM grid and allowed to settle for 2 min, after which the excess liquid was wicked away with

qualitative filter paper. Samples were then placed within centrifuge tubes and stored dry until the imaging session.

Stern-Volmer analysis on biliverdin nanoparticles

100 X stock metal salt solutions were prepared by dissolving each metal salt at a concentration of 230.6 mmol/mL. 10 X, 1 X, 0.1 X, and 0.01 X solutions were prepared by diluting the 100 X stock solutions. 500 µL of pH-adjusted biliverdin nanoparticle solution was placed in each 4-mL scintillation vial, and 50 µL of the corresponding metal chloride solution was added to each scintillation vial. Vials were shaken, after which the samples were protected from light and chelation was allowed to occur for 72 hours. Afterwards, absorbance and fluorescence spectra were collected for the samples.

Density Functional Theory

The chemical structures were initially energy optimized and the HOMO-LUMO surfaces were then calculated from their energy minimized geometries using a general ab initio quantum chemistry package, General Atomic and Molecular Electronic Structure System (GAMESS) program.[2] We used B3LYP functional while performing the density functional theoretical (DFT) calculations with 6-31G(d) as the basis set. Pople N31 was used for the polar groups. The highest occupied molecular orbital energy (E_{HOMO}), the lowest unoccupied molecular orbital energy (E_{LUMO}) and the energy gap between E_{LUMO} and E_{HOMO} was also calculated and represented as ΔE.

Single-particle Experiments and Analysis

Samples were prepared by drying 0.3 µL of diluted BVNP solutions on clean glass coverslips cleaned as done previously.[3] The coverslip was then kept in a clean biosafety cabinet for 10 min to allow the droplet to dry. All dilutions were made in degas-MiliQ water such that there were about 200 particles in single field of view. [4,5] A home-built, objective-based total internal reflection fluorescence microscopy (TIRFM) system was used for imaging single BV particles. A 100X oil immersion objective (100X, N.A. 1.49, oil immersion) was assembled on an inverted microscope. A 488-nm continuous wavelength laser was used as the light source and the power was set at 1.5mW at the back aperture of the objective. A neutral density filter of value 1 was placed in the path of light to control the amount of light going into the microscope. The incident light was directed through the objective via an exciter and a dual-band dichroic filter. Individual particles were seen as bright diffraction limited spots. The luminescence photons from individual BVNPs were collected by the same objective, passing an emitter and captured by an Electron Multiplying Charge Coupled Device (EMCCD) camera. A total of 1000 frames trajectory were acquired for each field of view with an integration time of 100 ms. At least four replicates were measured for each sample and was repeated for another batch of BVNPs.

A home-written script was used to extract the number of particles for each frame. The bleaching curve was generated by plotting the normalized number of particles versus time. The curve was then fitted with a two-component exponential function. The photobleaching lifetime was extracted from the fitted values. The BV signal (inside the boundary) and background (outside the boundary) were extracted by averaging a total of 100 by 100 pixels in the corresponding area. The net signal of BVs was calculated by subtracting the background from the gross BV signal for each frame. The emission decaying curve was generated by normalizing the maximum net BV signal to 1.0. A script was used to fit the normalized emission decaying curve with a two-component exponential function. The photobleaching lifetime was extracted from the fitted values ($\tau 1$ and $\tau 2$). The two time constants $\tau 1$ and $\tau 2$, as well as their respective weights and the goodness of fit (R2) were calculated using the following equation:

$$f(t) = ae^{\left(\frac{1}{r1}\right)\tau 1} + be^{\left(\frac{1}{r2}\right)\tau 2}$$

Because the variance of the data is larger at the longer timescale than at the shorter timescale, the "Weighted Least Square" fit option was used and each data point was weighted by its variance. Single-particle trajectories were segmented to define the "on" and "off" states based on changepoint analysis.[6,7] The intensity threshold was defined as the mean of the segment with the lowest intensity plus three times the standard deviation of that segment. A segment of the trajectory whose intensity was above this threshold is defined as an "ON" state and its duration as t_{on}. An "OFF" state refers to any segment whose intensity was below the threshold and its duration as t_{off}. An array of t_{on} and t_{off} was collected from each trajectory and pooled for the same type of particle. The power-law distribution of t_{on} and t_{off} were generated by plotting the histogram of pooled data.

Figures

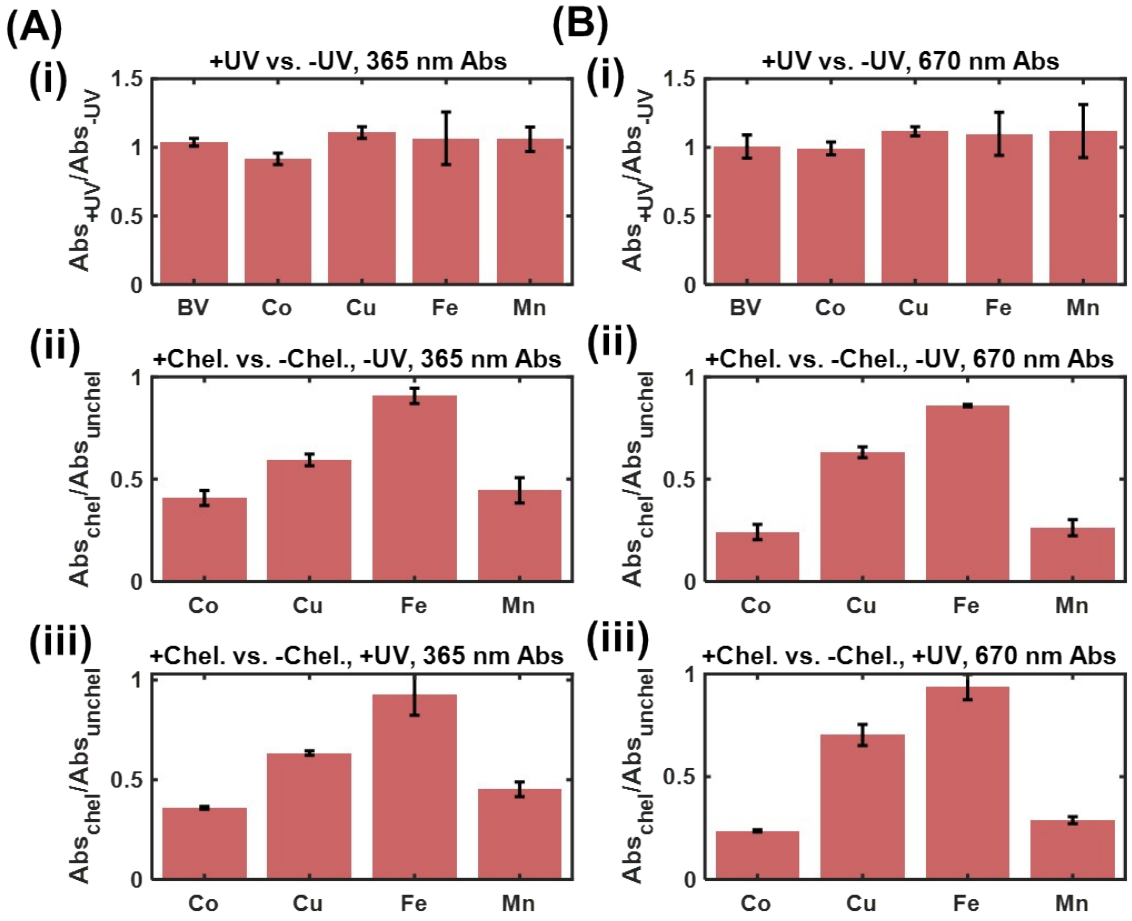

Figure S1. Absorbance ratios for BV. Error bars represent standard deviation across two separate experiments. **(A)** Ratio of 365 nm absorbance for samples **(i)** with and without UV irradiation, **(ii)** with and without metal chelation when no UV irradiation was used, and **(iii)** with and without metal chelation when UV irradiation was used. **(B)** Ratio of 680 nm absorbance for samples **(i)** with and without UV irradiation, **(ii)** with and without metal chelation when no UV irradiation was used, and **(iii)** with and without metal chelation when UV irradiation was used.

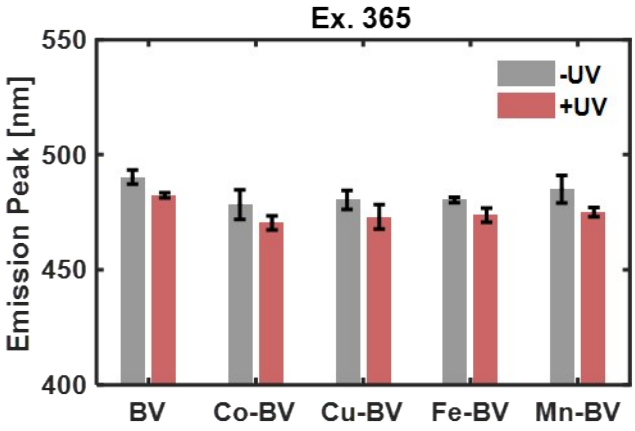

Figure S2. Wavelength of maximum fluorescence (ex. 365 nm) for BV samples before and after UV irradiation. Error bars represent standard deviation obtained with three separate experiments.

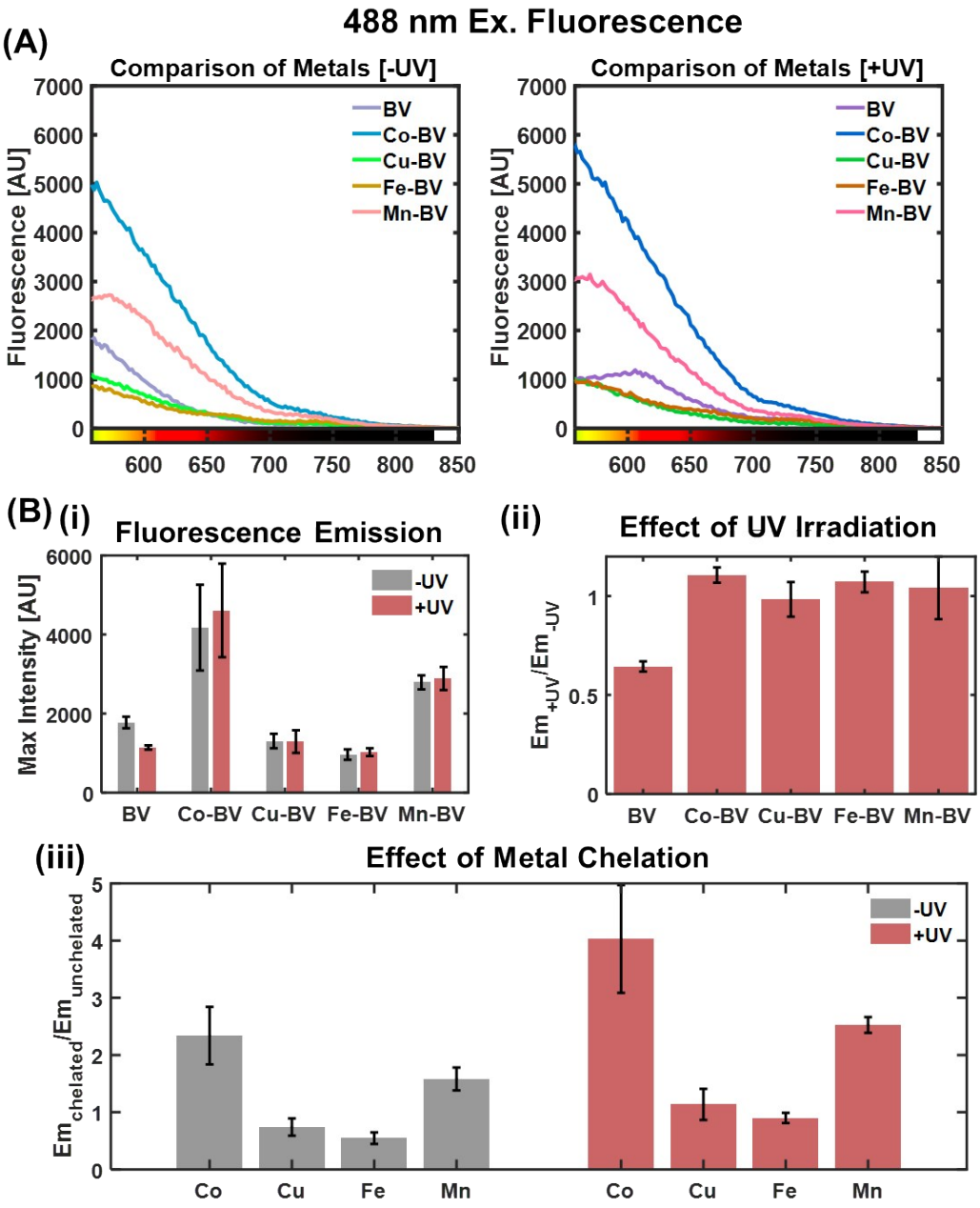

Figure S3. Fluorescence behavior of BV for 488 nm excitation. **(A)** Fluorescence spectra of BV samples without UV irradiation and after 72 h of UV irradiation. An excitation wavelength of 488 nm and gain of 150 was used. **(B)** Average fluorescence for 488 nm excitation. Error bars represent standard deviation across three separate experiments. **(i)** Average fluorescence intensity for BV with and without 72 h UV irradiation. **(ii)** Average ratio of fluorescence intensity with UV irradiation to fluorescence intensity without UV irradiation. **(iii)** Average ratio of fluorescence intensity with metal chelation to fluorescence intensity without metal chelation, in the absence of UV irradiation. **(iv)** Average ratio of fluorescence intensity with metal chelation to fluorescence intensity without metal chelation, after 72 h UV irradiation.

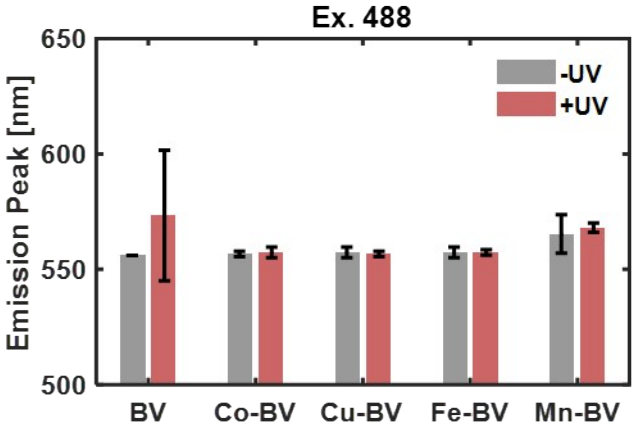

Figure S4. Wavelength of maximum fluorescence (ex. 488 nm) for BV samples before and after UV irradiation. Error bars represent standard deviation obtained with three separate experiments.

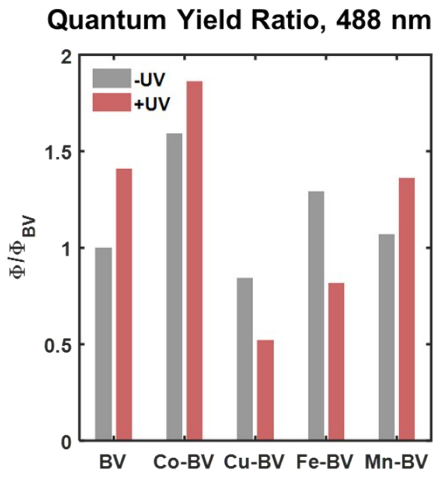

Figure S5. 488 nm quantum yield expressed as a ratio to that of BV.

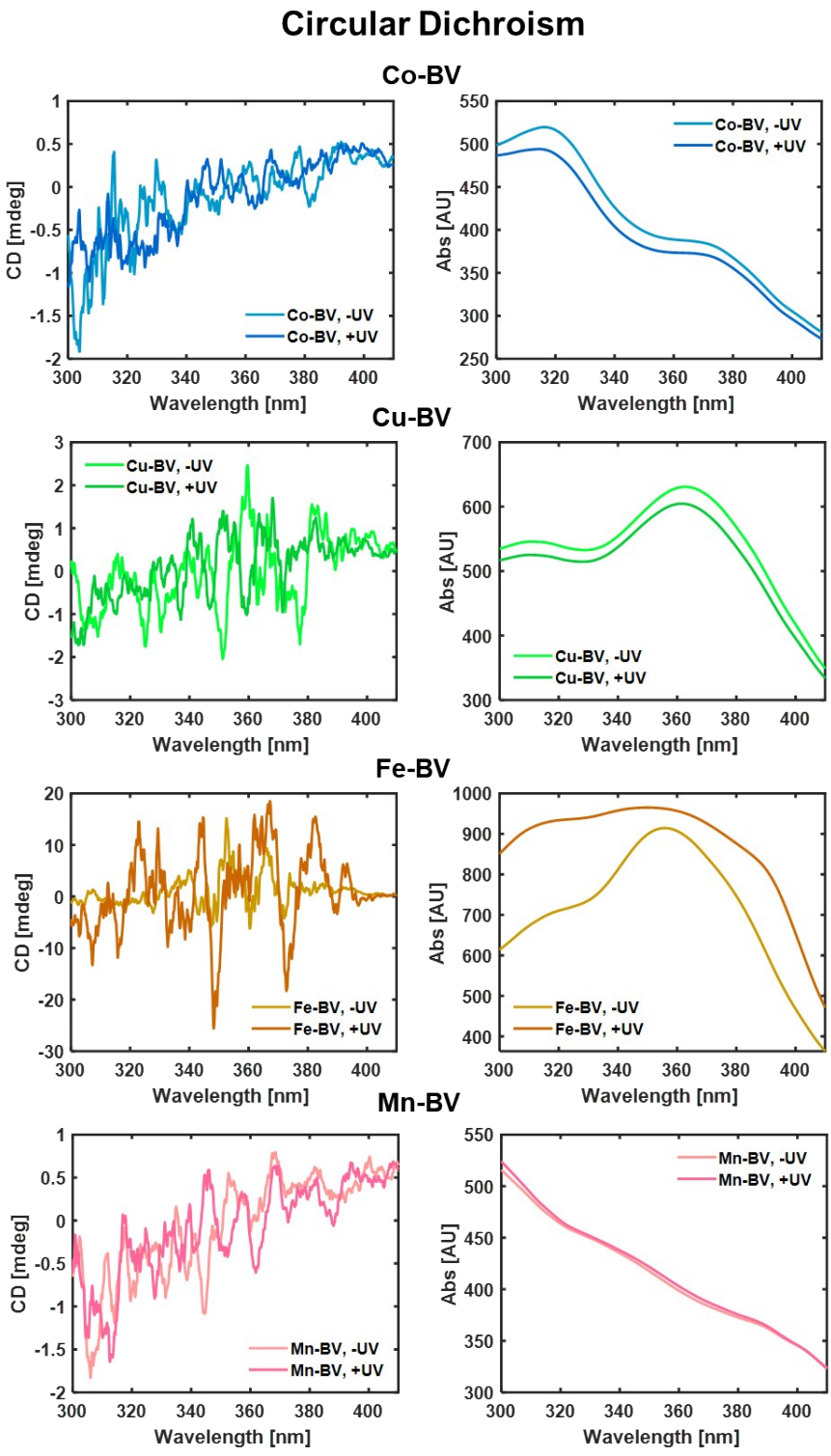

Figure S6. Circular dichroism spectra of biliverdin-metal chelates.

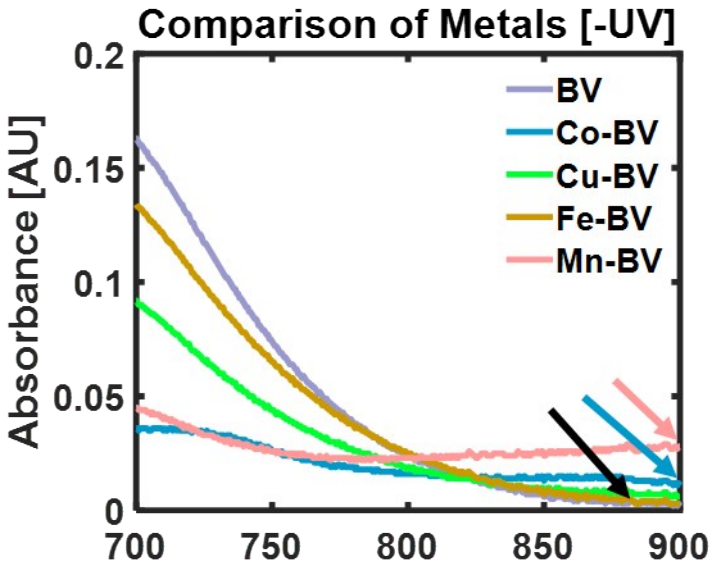

Figure S7. UV-Visible spectra of metal-chelated BV (in comparison to BV) without UV irradiation, in the range of 700 to 900 nm. Arrows indicate approximate locations of starting wavelengths for the compounds (The black arrow represents approximate beginning of BV, Cu-BV, and Fe-BV peaks, while the pink and blue arrows match the colors of their respective spectra).

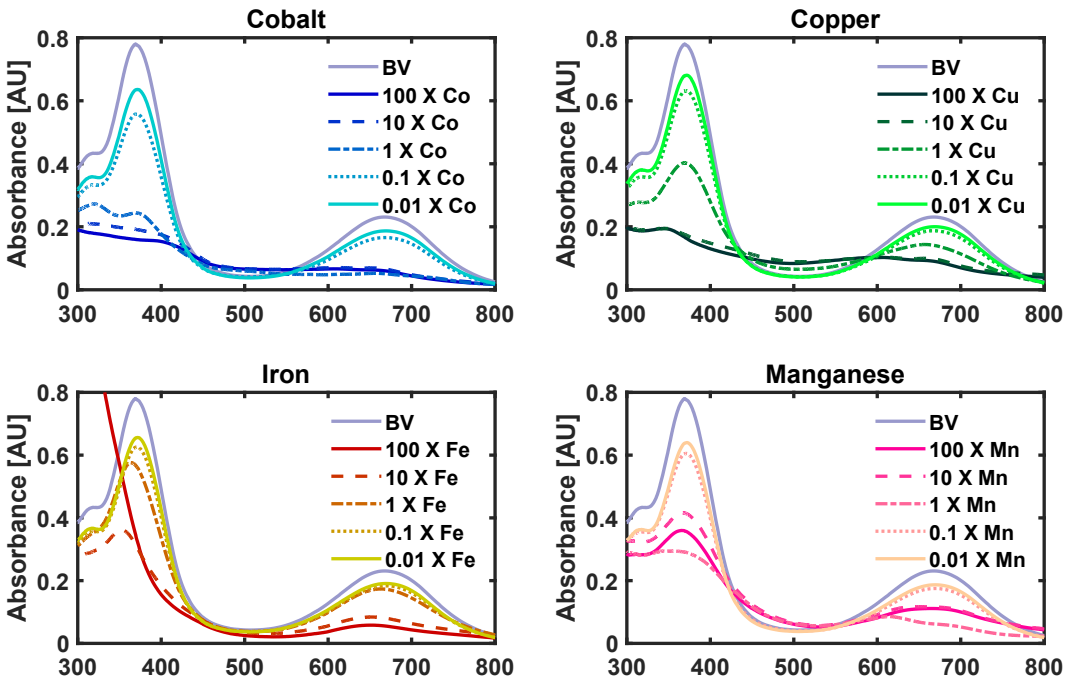

Figure S8. Absorbance curves of BV and metal-chelated BV at different metal concentrations.

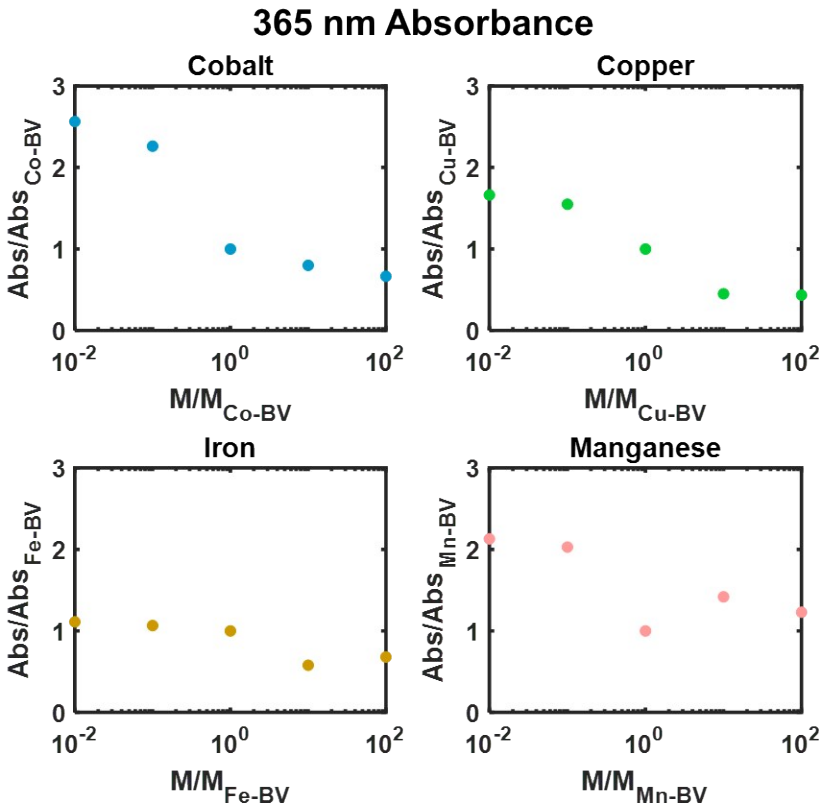

Figure S9. 365 nm absorbance of various metal concentrations expressed as a ratio to that of the 1 X metal concentration. Higher metal concentrations generally lead to lower 365 nm absorbance.

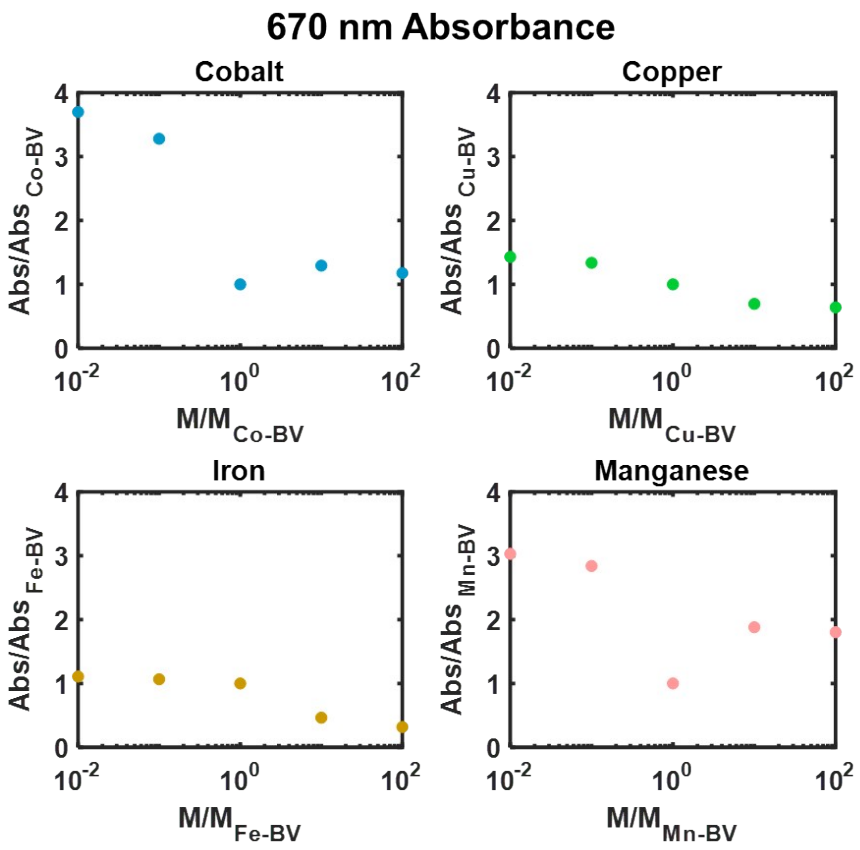

Figure S10. 670 nm absorbance of various metal concentrations expressed as a ratio to that of the 1 X metal concentration. Higher metal concentrations generally led to decreased 670 nm absorbance.

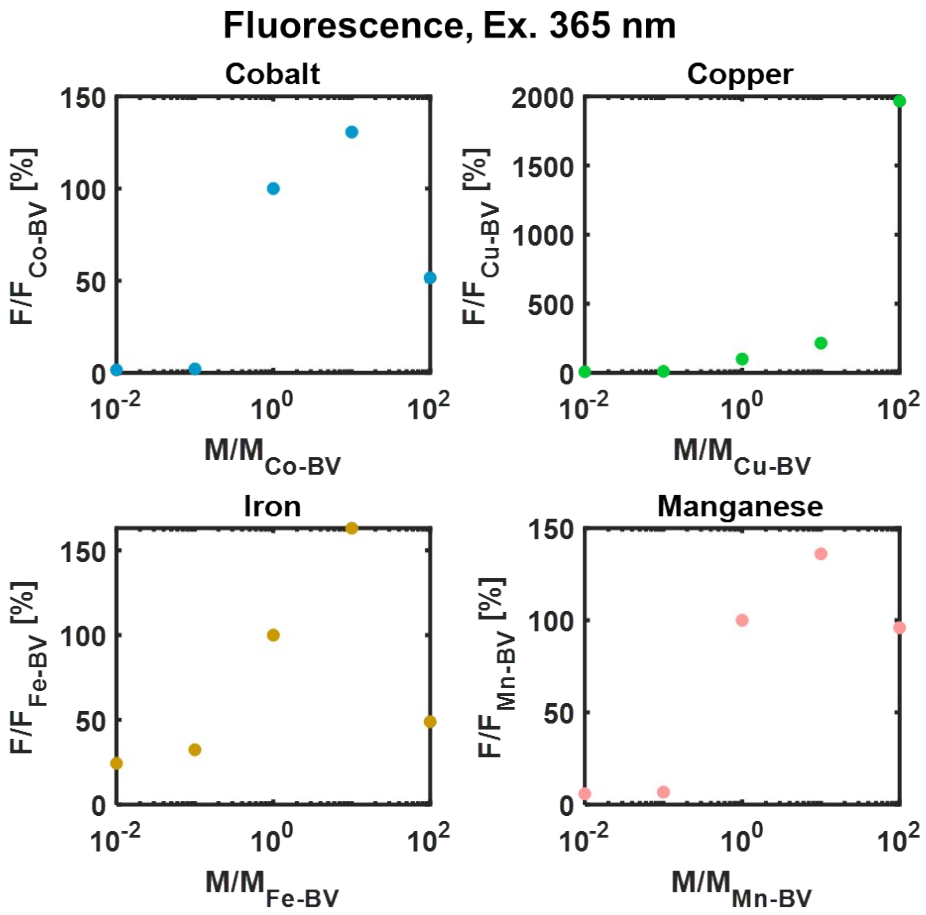

Figure S11. Maximum fluorescence emission intensity (for 365 nm excitation) of various metal concentrations expressed as a percentage of the intensity at the 1 X metal concentration. Fluorescence is dependent on the metal concentration, with increasing concentration generally leading to an increase in fluorescence intensity.

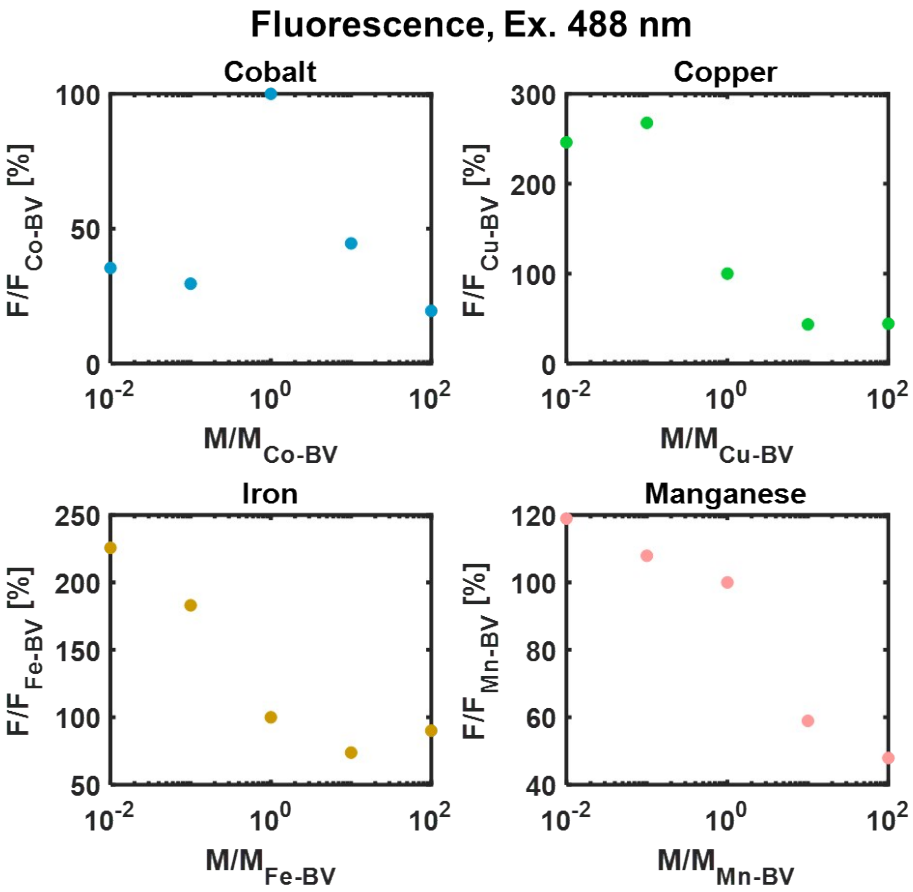

Figure S12. Maximum fluorescence emission intensity (for 488 nm excitation) of various metal concentrations expressed as a percentage of the intensity at the 1 X metal concentration. Fluorescence is dependent on the metal concentration, with increasing concentration generally leading to a decrease in fluorescence intensity.

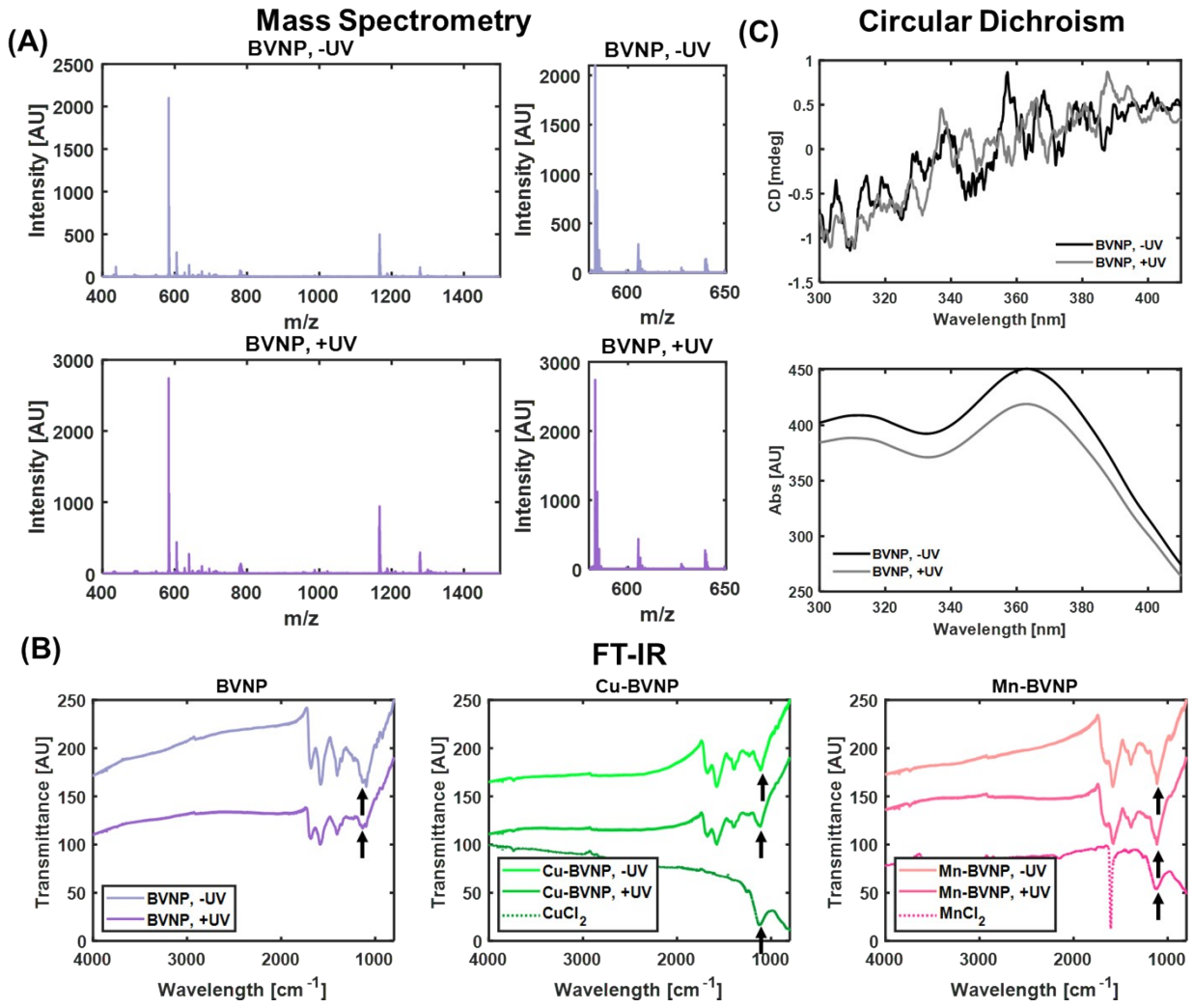

Figure S13. BVNP stability and conformational change. **(A)** Mass spectra of BVNP without UV irradiation and after 72 h of UV irradiation. The presence of expected characteristic peaks and lack of appearance of new peaks of smaller masses indicates BVNPs are not degrading as a result of the UV irradiation. **(B)** FT-IR spectra of BVNP and BVNP metal chelates. Black arrows identify peaks that are altered as a result of metal chelation. There is no apparent change as a result of UV irradiation. **(C)** Circular dichroism spectra of UV irradiation does not appear to have a noticable effect on the CD spectra. The magnitude of BVNP CD spectra is lower than that of BV.

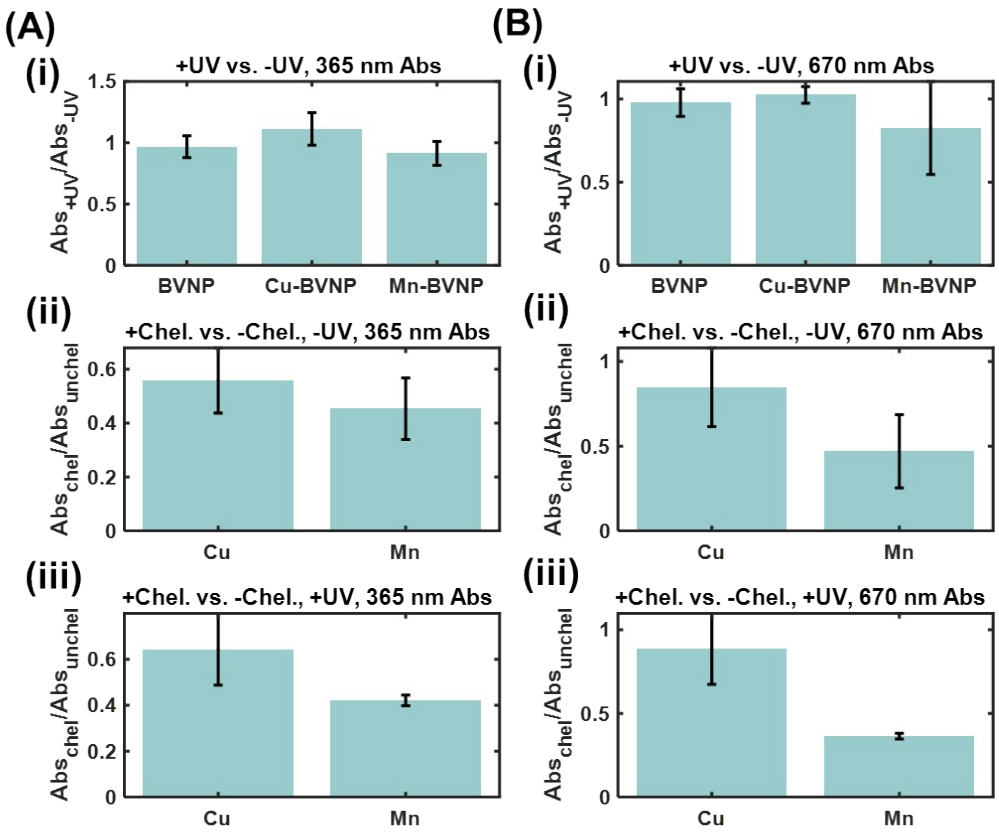

Figure S14. Absorbance ratios for BVNPs. Error bars represent standard deviation across two separate experiments. **(A)** Ratio of 365 nm absorbance for samples **(i)** with and without UV irradiation, **(ii)** with and without metal chelation when no UV irradiation was used, and **(iii)** with and without metal chelation when UV irradiation was used. **(B)** Ratio of 680 nm absorbance for samples **(i)** with and without UV irradiation, **(ii)** with and without metal chelation when no UV irradiation was used, and **(iii)** with and without metal chelation when UV irradiation was used.

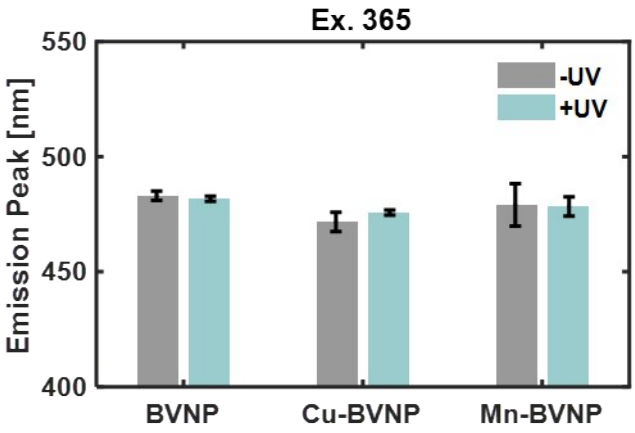

Figure S15. Wavelength of maximum fluorescence (ex. 365 nm) for BVNP samples before and after UV irradiation. Error bars represent standard deviation obtained with three separate experiments.

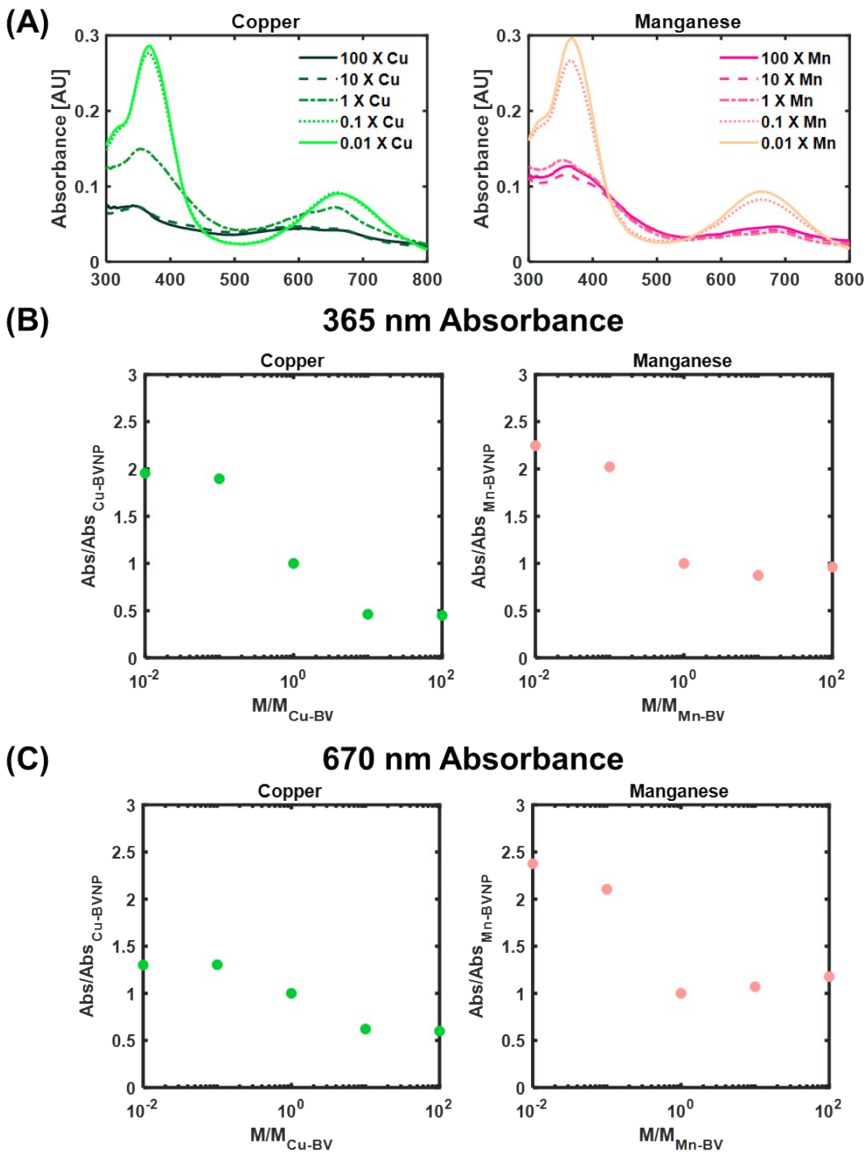

Figure S16. Absorbance behavior of metal-chelated BVNP at different metal concentrations. **(A)** UV-visible spectra with multiple metal concentrations. **(B)** 365 nm absorbance of metal-chelated BVNPs expressed as a ratio to that of 1 X metal chelated BVNPs. **(C)** 670 nm absorbance of metal-chelated BVNPs expressed as a ratio to that of 1 X metal chelated BVNPs.

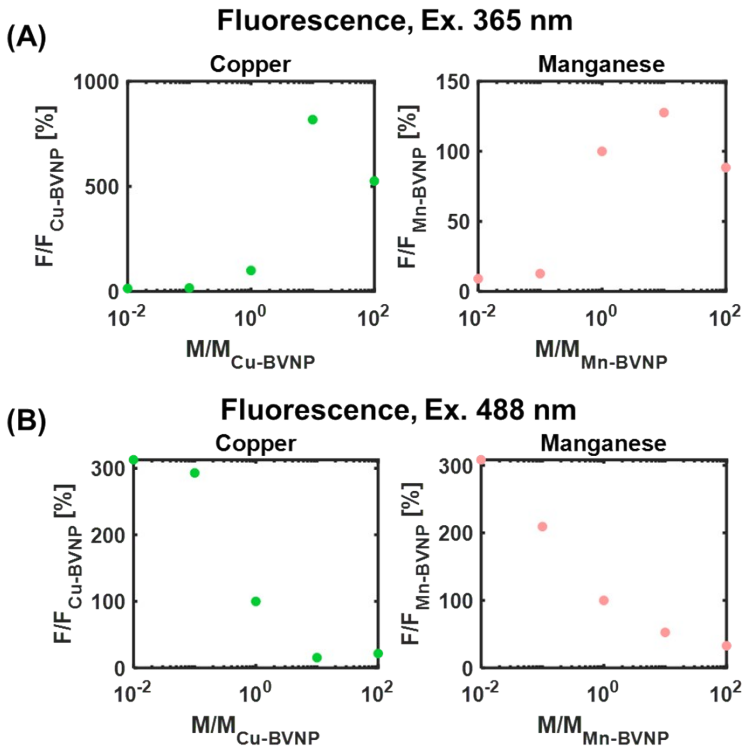

Figure S17. Maximum fluorescence emission intensity of BVNPs chelated with various metal concentrations expressed as a percentage of the intensity at the 1 X metal concentration. **(A)** 365 nm excitation. **(B)** 488 nm excitation.

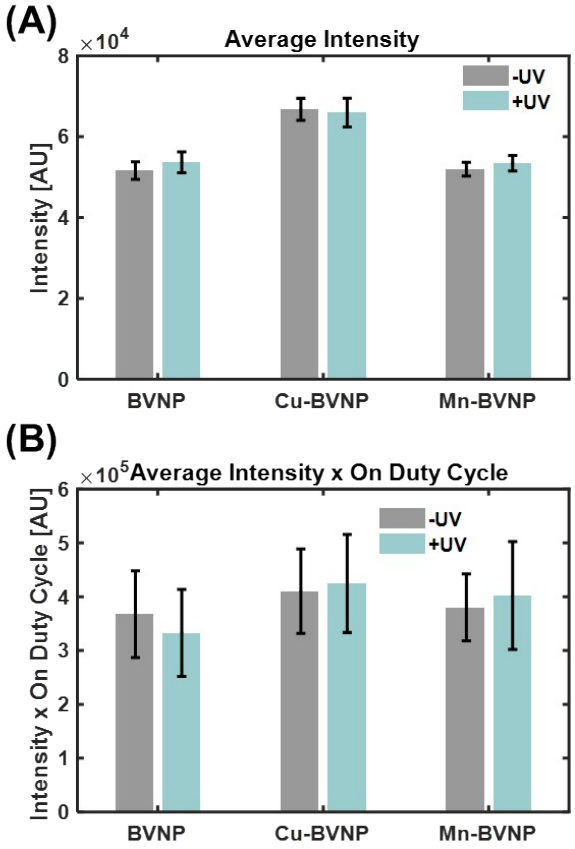

Figure S18. Single-particle brightness of BVNPs. Error bars represent standard deviation of measurements from multiple individual particles. **(A)** Average single-particle intensity of BVNP, Cu-BVNP, and Mn-BVNP, with and without UV irradiation. **(B)** Product of average single-particle intensity and on-time duty cycle for BVNP, Cu-BVNP, and Mn-BVNP.

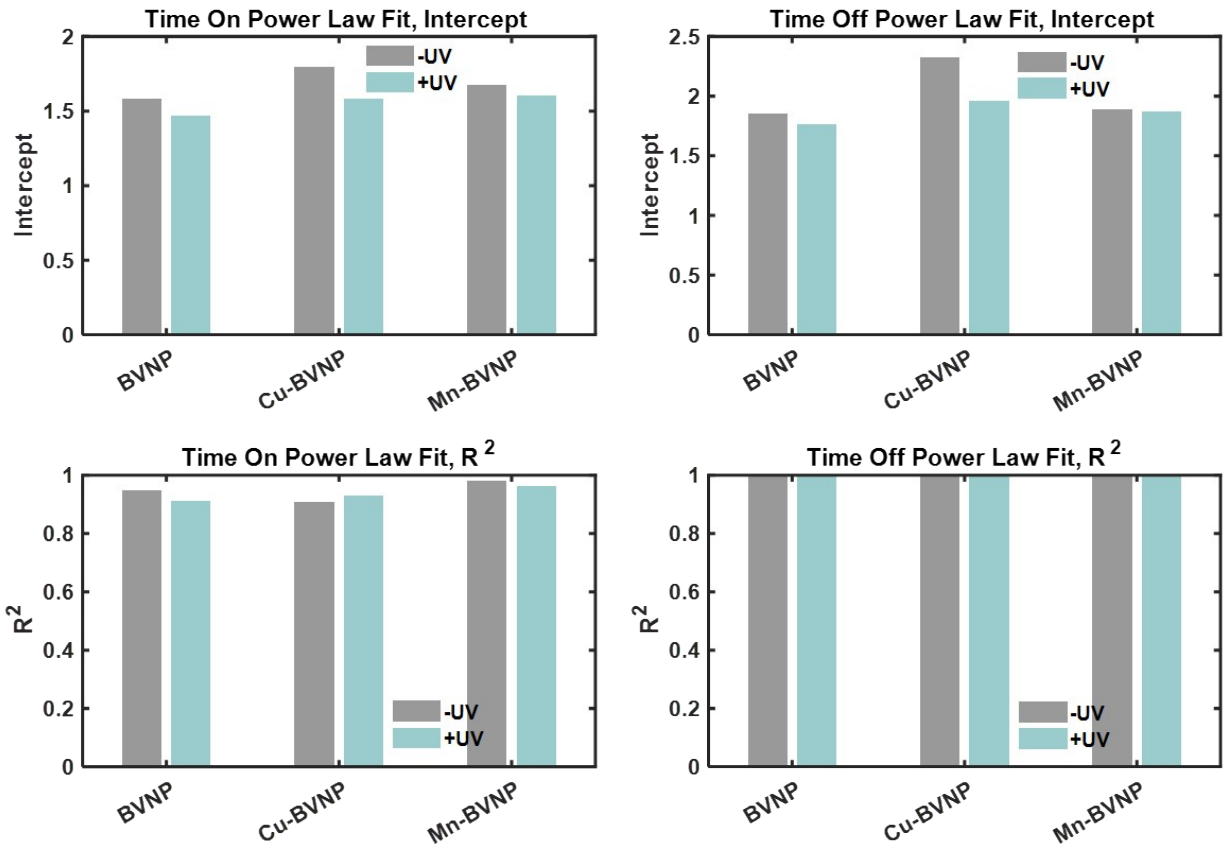

Figure S19. Time on and time off power law fit intercepts and R^2 values.

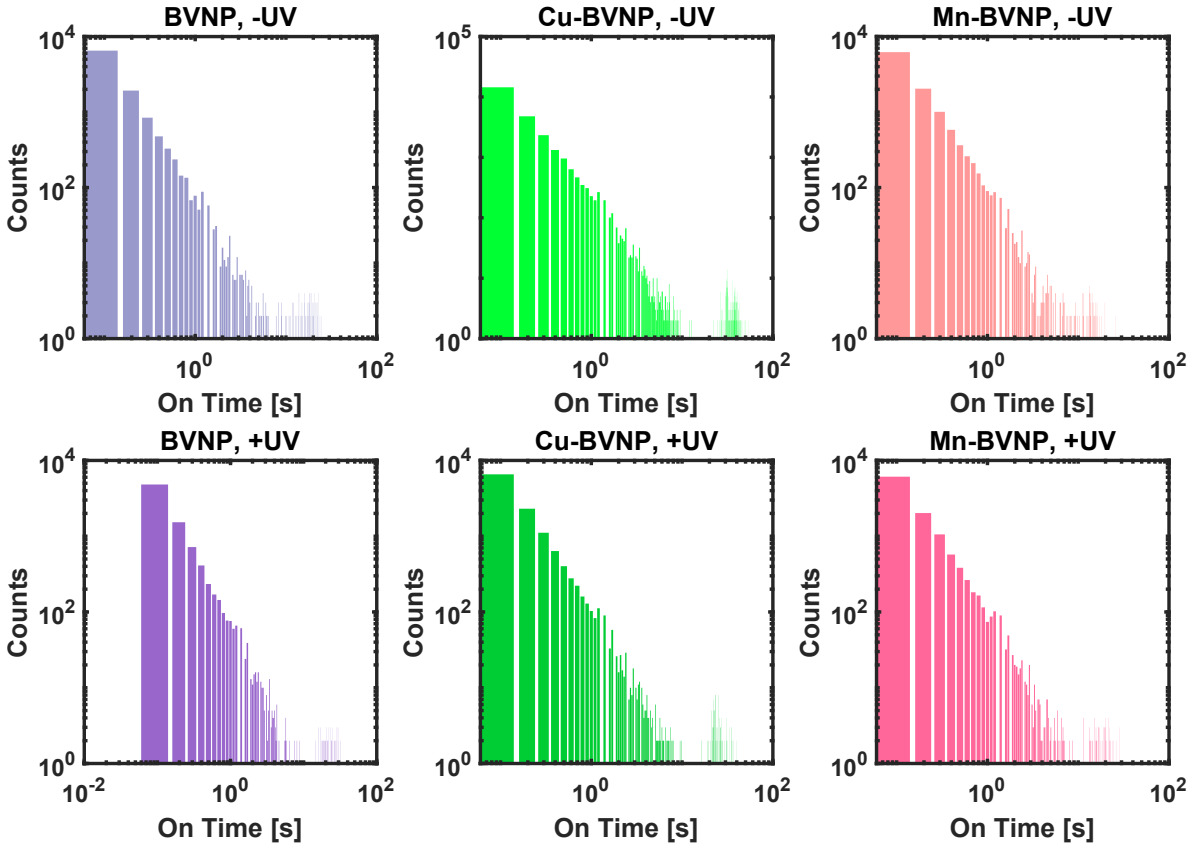

Figure S20. Log-log histograms of counts as a function of on time.

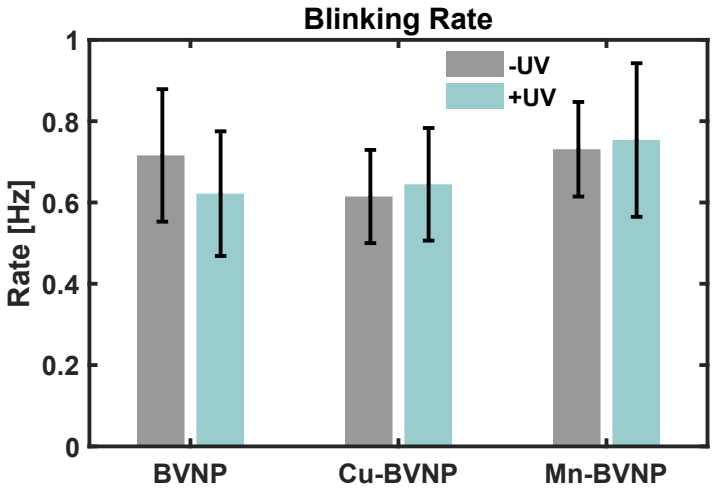

Figure S21. Single-particle blinking rate. Error bars represent standard deviation of measurements from multiple individual particles.

References

1 I. Goncharova and M. Urbanová, *Anal. Biochem.*, 2009, **392**, 28–36.

2 M. W. Schmidt, K. K. Baldridge, J. A. Boatz, S. T. Elbert, M. S. Gordon, J. H. Jensen, S. Koseki, N. Matsunaga, K. A. Nguyen, S. Su, T. L. Windus, M. Dupuis and J. A. Montgomery, *J. Comput. Chem.*, 1993, **14**, 1347–1363.

3 T. Camp, K. Mehta, S. G. Sligar and K. Zhang, *Anal. Chem.*, 2020, **92**, 2229–2236.

4 S. K. K. Misra, I. Srivastava, J. S. Khamo, V. V Krishnamurthy, D. Sar, A. Schwartz-Duval, J. Soares, K. Zhang and D. Pan, *Nanoscale*, , DOI:10.1039/C8NR04065F.

5 P. Fathi, J. S. Khamo, X. Huang, I. Srivastava, M. B. Esch, K. Zhang and D. Pan, *Carbon N. Y.*, 2019, **145**, 572–585.

6 L. P. Watkins and H. Yang, *J. Phys. Chem. B*, 2005, **109**, 617–628.

7 D. Montiel, H. Cang and H. Yang, *J. Phys. Chem. B*, 2006, **110**, 19763–19770.